

Portland State University

PDXScholar

Geology Faculty Publications and Presentations

Geology

1984

Igneous Dikes at Long Valley, CA: Emplacement Mechanisms and Associated Geologic Structures

David D. Pollard
Stanford University

Jonathan H. Fink
Portland State University, jon.fink@pdx.edu

Paul T. Delaney
U.S. Geological Survey

Follow this and additional works at: https://pdxscholar.library.pdx.edu/geology_fac



Part of the [Geology Commons](#), and the [Volcanology Commons](#)

Let us know how access to this document benefits you.

Citation Details

Pollard, D. D., Fink, J. H., & Delaney, P. T. (1984). Igneous dikes at Long Valley, CA; emplacement mechanisms and associated geologic structures. In Proceedings of Workshop XIX (pp. 130-146).

This Conference Proceeding is brought to you for free and open access. It has been accepted for inclusion in Geology Faculty Publications and Presentations by an authorized administrator of PDXScholar. Please contact us if we can make this document more accessible: pdxscholar@pdx.edu.

IGNEOUS DIKES AT LONG VALLEY, CA: EMPLACEMENT MECHANISMS AND ASSOCIATED GEOLOGIC STRUCTURES

David D. Pollard
Dept. of Applied Earth Sciences
Stanford University
Stanford, CA 94305

Jonathan H. Fink
Dept. of Geology
Arizona State University
Tempe, AZ 85287

Paul T. Delaney
U.S. Geological Survey
2255 N. Gemini Drive
Flagstaff, AZ 86001

Abstract

Two hypotheses for dike emplacement are: (1) magma flows into and dilates pre-existing fractures; or (2) magma flows into and dilates self-generated fractures. In the first case dikes should be parallel to an element of the rock fabric; in the second, they should be perpendicular to the least compressive stress. The two hypotheses suggest different dike intrusion and fissure eruption mechanisms and therefore different strategies for monitoring igneous events at Long Valley. We derive a method to distinguish the two mechanisms, a priori, from in-situ stress measurements and estimates of magma pressure. Estimates of relative dilation and slip across a dike plane from models constrained by surface displacement data provide a method to distinguish the two mechanisms, a posteriori. Joints cluster near dike contacts just as microcracks cluster near laboratory fractures. Such clusters define a process zone of secondary cracking that forms at the tip of a primary crack. For basaltic dikes in sedimentary host rocks of the Colorado Plateaus, the process zone size is about 10 m and the number of joints is in the range 10 to 100. The mechanical energy release rate for propagation of these dikes is estimated to be 10 to 100 times that for a single laboratory fracture. Data from proposed drill holes through rhyolite dikes under the Inyo Domes will elucidate propagation mechanisms and process zone characteristics. As a dike nears the Earth's surface, two sets of ground cracks open parallel to the dike trend. A "rule of thumb" is that the depth to the dike top is one-third to one-half the spacing between the innermost surface cracks of each set. Surface structures on and near the Inyo Domes suggest a NNE trend for shallow (< several hundred meters) dike segments, but dome alignment suggests a NNW trend for the feeder dikes at depth.

Introduction

Recent geophysical surveys (Steeple and Iyer, 1976; Hill, 1976; Sanders and Ryall, 1983) provide evidence for a magma reservoir beneath Long Valley Caldera. Geodetic measurements between 1975 and 1980 can be interpreted as an inflation of this reservoir under the resurgent dome of the caldera (Savage and Clark, 1982). Knowledge that the crust beneath Long Valley is pervaded by steeply-dipping faults, joints, and other planes of weakness (Bailey and Koeppen, 1977; Bailey et al., 1976) invites the hypothesis that magma from an inflating reservoir could flow into some of these pre-existing fractures, dilate them to form an igneous dike, and thereby establish a conduit that could transport magma to the surface. In this case, dike orientation is controlled by the pre-existing fractures, a relationship that has been advocated for numerous geologic settings (e.g. Wilson, 1970).

A contrasting emplacement hypothesis is that dike dilation generates sufficient tension in the host rock ahead of the dike tip to create new fractures, into which the magma may flow (Anderson, 1938). These fractures and the subsequent dike will be oriented perpendicular to the direction of least compressive stress. This obviates the need for pre-existing fractures and generates a dike orientation that is controlled by the state of stress. If the least compressive stress is subhorizontal, such dikes will be steeply-dipping and capable of transporting magma to the surface.

The two hypotheses for dike propagation admit different deductions about the relations among dike attitude, rock fabric, and tectonic stress orientation and suggest different fissure eruption mechanisms. If propagation along pre-existing fractures is the appropriate mechanism, then geological mapping and geophysical surveying of the rock fabric (fractures, faults, joint sets, etc.) will provide valuable data for forecasting likely locations of dikes and fissures. Three criteria must be

satisfied for this mechanism to be viable: the magma must find access to the fracture; it must be able to dilate the fracture; and it must flow a significant distance along the fracture. For dilation to occur magma pressure must exceed the compressive stress acting across the plane of the fracture. However, this compressive stress need not be a principal stress, so the directions of the principal stresses acting at the time of intrusion need bear no unique relation to the pre-existing fracture or the dike.

In contrast, if dike propagation along self-generated fractures is the appropriate fissure eruption mechanism, then measurement of the stress (or strain) field is crucial for monitoring and forecasting because of the unique relationship between orientations of dikes and principal stresses. This relationship has been exploited successfully to estimate paleostress directions from ancient dikes (e.g. Nakamura, 1977; Zoback and Zoback, 1980; Bacon et al., 1980; Delaney and Pollard, 1981). The inverse procedure could be used to interpret in situ stress measurements and geodetic (strain) data from Long Valley in order to forecast likely orientations of dikes and eruptive fissures.

Geophysical and structural geologic criteria are needed to distinguish between the two hypotheses and to establish which might be appropriate at Long Valley. In this paper we discuss several aspects of the rise of magma from a reservoir through dikes to the surface, including deformation and structures likely to develop at each stage of emplacement. We indicate which of these features might be detected at Long Valley, and which might be used to interpret data obtained from a drilling program such as that currently underway at the nearby Inyo Domes.

Relations Among Dike Attitude, Rock Fabric, and Tectonic Stress

In order for a dike to be emplaced along a steeply dipping plane of weakness (fracture), the magma pressure P_m must exceed the subhorizontal compressive

stress acting across that plane. Delaney et al. (in prep.) have used this necessary condition for dike dilation to relate the state of stress to dike attitude. The remote least compressive stress σ_1^r is subhorizontal, but of arbitrary orientation α relative to the normal to the fracture plane (Fig. 1, inset). The other subhorizontal principal stress σ_2^r may be the intermediate or maximum compressive stress. Tensile stress is taken as positive, and a ratio of stresses \underline{R} is defined as

$$\underline{R} = (\sigma_1^r + \sigma_2^r + 2\underline{P}_m) / (\sigma_1^r - \sigma_2^r)$$

The condition defines two regions on Figure 1, a graph of stress ratio \underline{R} versus angle α . For combinations of \underline{R} and α falling in the lower area, dilation is impossible and therefore magma cannot invade the fracture. In the upper area dilation is possible, so a dike may form if the magma finds access to the fracture and if it can flow a significant distance before stagnating (Delaney and Pollard, 1982).

To apply this condition we must estimate the stress ratio \underline{R} . The magnitude of the magma pressure is estimated as $\underline{P}_m = \underline{\gamma}_m \underline{d}$ where $\underline{\gamma}_m$ is the unit weight of the magma and \underline{d} is depth. The principal regional stresses are estimated as $\sigma_1^r = -\underline{m} \underline{\gamma}_r \underline{d}$ and $\sigma_2^r = -\underline{n} \underline{\gamma}_r \underline{d}$ where $\underline{m} < \underline{n}$ are constants determined by the tectonic regime, $\underline{\gamma}_r$ is the unit weight of the rock, and we set $\underline{\gamma}_m \approx \underline{\gamma}_r$. Based on in situ measurements described by McGarr (1982), the ratio \underline{R} may be about +1 in some extensional tectonic regimes because $\underline{m} \approx .5$ and $\underline{n} \approx 1$. \underline{R} may be about -1 in some contractional tectonic regimes because $\underline{m} \approx 1$ and $\underline{n} \approx 1.5$.

If Long Valley were considered to be in a contractional regime, Figure 1 suggests that magma could not easily invade planes of weakness, even those at small angles α , so dike orientation and principal stress planes should coincide. In contrast, if Long Valley is representative of an extensional regime, the stress directions may not be indicative of potential dike orientations. Rather, the rock

fabric may control dike orientation because planes of weakness at large angles α can be dilated. Additional data on the state of stress and magma pressure in the Long Valley region are needed to refine this analysis and to ascertain whether knowledge of the stress ratio \underline{R} can be used to distinguish the two emplacement hypotheses.

Relations Among Dike Attitude, Dilation, and Slip

Shear stresses act across all planes of weakness not oriented in a principal stress plane. These shear stresses will not generate slip (faulting) if there is sufficient frictional resistance along the plane. However, if magma invades a plane of weakness, frictional resistance is removed and the shear stress will be relaxed by a shear displacement \underline{u}_2 , that accompanies the dilational displacement \underline{u}_1 (Fig. 2, inset). Thus, detection of slip across eroded dikes by geologic mapping is an indication that the dike may not have been emplaced along a principal stress plane. Of course it must be demonstrated that the slip and dilation were contemporaneous.

To quantify relations among dike attitude, dilation, and slip, the ratio of these displacements at the center of a dilating plane of weakness is plotted versus angle α in Figure 2 using the stress ratio \underline{R} as a parameter. For $\underline{R} > 10$ (a condition produced by relatively great magma pressure and/or a small difference between the remote principal stresses), the displacement ratio is less than 0.1 for all α . That is, slip will be insignificant (and perhaps not measureable) relative to dilation no matter what the dike attitude was relative to the principal stresses. Clearly, the displacement ratio will not be a good criterion for distinguishing the emplacement hypotheses under these conditions. However, for smaller values of \underline{R} the displacement ratio can be large, approaching unity for small angles α . Thus, where magma pressure is not great relative to the regional stresses and/or the

regional stress difference is large, the two hypotheses should be distinguishable.

For modern dike emplacement events, displacement usually cannot be measured at the buried dike contact. On the other hand, geodetic measurements record surface displacements that, in some instances, are known to have been caused by dike emplacement (Pollard et al., 1983). Such surface displacements can be used to constrain models from which one infers the displacement ratio at the dike contact. Model results of geodetic measurements at Long Valley indicate combinations of slip and dilation on planes at depth (Savage and Cockerham, 1984). This is consistent with dike emplacement along pre-existing planes of weakness that are not symmetric to the principal stresses. An alternate model (Rundle and Whitcomb, 1984) provides an adequate fit to the geodetic data using point sources of dilation (magma reservoirs) rather than slipping and dilating surfaces (faults and dikes). Apparently, the two subsurface configurations cannot be distinguished unambiguously using these geodetic data. However, additional data and model studies are indicated because the technique is sound in principle, and it provides one of the most direct measures of subsurface deformation.

Fractures Formed in the Process Zone of a Dike

Dike emplacement and propagation involves several complex processes, some of which are illustrated in Figure 3. Here we focus on the possible development of fractures near the dike tip. In so far as dikes act like pressurized cracks (Pollard, 1973), we may employ the methods of linear elastic fracture mechanics (Lawn and Wilshaw, 1975), to show that the stress field near the dike tip involves a concentration of tensile stress that could promote the formation of vertical joints (Delaney et al., in prep.). The region of jointing at the dike tip is analogous to the process zone of microcracking at the tip of a small fracture in rock (Hoagland et al., 1973). These joints, if present, will affect the cooling history of the intrusion

and local hydrothermal circulation. They will weaken the host rock and provide a pathway for flow of the magma, thus satisfying the second emplacement hypothesis. Surface exposures of igneous dikes are rare in the Long Valley area. However, slant drill holes are planned to penetrate the inferred dike below the vent area of one of the Inyo Domes during Autumn of 1984. Observations of joints and other fractures near this dike will elucidate the propagation mechanism.

Stresses near the dike tip are proportional to the square root of dike half-height divided by radial distance from the tip, $(a/r)^{1/2}$ (Lawn and Wilshaw, 1975). It is also proportional to the difference between the magma pressure and regional compressive stress acting across the dike plane, $(P_m - S)$. This driving pressure is a quantity about which we know very little. Nonetheless, we use an estimate of 1 to 10 MPa for the driving pressure and employ the criterion that the induced tensile stress must nullify the ambient compression ($S > 50$ MPa for depths > 2 km) and then exceed the tensile strength (1 to 10 MPa) of the host rock. This criterion leads to an estimate of the distance from the tip over which joints might form that ranges up to 0.01 times the dike height. For a dike from 1 to 10 km high the analysis suggests that joints might form at distances as great as 10 to 100 m from the tip. Drill hole observations will provide a direct measure of this distance.

The concentrated horizontal tensile stress σ_{11} (Fig. 4, inset) does not reach a maximum on the extension of the dike plane. Instead, two maxima exist on either side of the dike plane. This is illustrated in Figure 4, a graph of the horizontal stress induced by dike dilation normalized by driving pressure and plotted versus distance perpendicular to the dike plane. Distance above the dike tip is used as a parameter and all distances are normalized by dike half-height a . We suggest that vertical joints (Fig. 4, inset) form in response to these tensile maxima. This stress distribution provides an explanation for the formation of joints on either side of the

plane of a dike. As dike propagation continues, the joint set formed in this manner is bisected and the joints become adjacent to the dike contact.

Sedimentary rocks outcropping near mafic dikes of the Colorado Plateaus province commonly display a systematic joint set parallel to those dikes (Delaney, et al., in prep.). At some localities a distinctive set of dike-parallel joints is spatially restricted to distances from the contact that are a small fraction of dike length or height. Spacing of these joints increases with distance from the contact. A map (Fig. 5) of an outcrop of Jurassic Summerville Formation west of the San Rafael Monocline in south-central Utah shows a set of joints adjacent to a northerly-striking diabase dike. The dike-parallel set truncates a younger, northeasterly-striking set of joints that is unrelated to the igneous event. The dike-parallel set is not found more than 10 m from the contact. Outcrops like that in Figure 5 and the analysis mentioned above have persuaded us that joint formation near a dike tip is common and important.

The formation of numerous microcracks in the process zone of a small fracture in laboratory specimens of rock increases the amount of energy required for the fracture to propagate by one to two orders of magnitude over that required for a single microcrack in a mineral grain (Friedman et al., 1972). We suggest that each joint of a dike-parallel, adjacent set is similar to the laboratory fracture. Therefore, the formation of multiple joints in the process zone of a dike would increase the energy required for dike propagation over that for the single fracture. Because there typically are 10 to 100 dike-parallel joints, we would expect the mechanical energy release rate to be one to two orders of magnitude greater for dike propagation than for laboratory fracture propagation under similar conditions.

Surface Cracking and Faulting Over a Dike

As a propagating dike nears the Earth's surface, the tensile stress concentra-

tion above its tip spreads outward and upward, intersecting the surface at two points to form secondary stress maxima (Fig. 6). The direction of maximum tension at the surface is horizontal and perpendicular to the strike of the dike. Patterns of open ground cracks and steeply-dipping normal faults can be related to this stress distribution above dikes (Pollard, et al., 1983; Fink and Pollard, 1983a). In general the secondary maxima will produce these extensional structures in two linear clusters that align with the strike of the dike and straddle the ground through which a fissure eruption may occur. The middle ground is subject to smaller tensile stresses and therefore may not crack or fault. However, this ground may be dropped down along flanking normal faults to form a graben. Beyond the two tensile maxima the stress decreases and small compressive stresses are induced at a distance somewhat greater than the depth to the dike center.

A "rule of thumb" for estimating the depth to a dike top has been derived and is illustrated in Figure 7. The spacing w between positions of maximum tension is plotted on this graph versus the depth to the dike top ($d - a$). Both lengths are normalized by the depth-to-center of the dike d . As the dike tip propagates upward from a fixed central depth the spacing decreases. We suggest that surface cracks form near the position of the maximum tensile stress if it is of sufficient magnitude to overcome the tensile strength of the surficial material. The "rule" indicates that the depth to the dike top falls in the range between one third and one half of the spacing between the innermost set of surface cracks.

Preliminary mapping (Fig. 8) of cracks and faults along the trend of the Inyo Domes suggests the presence of a dike underlying and parallel to the domes. Two series of prominent earth cracks (Benioff and Gutenberg, 1939) define a graben approximately 1.5 km wide which extends north from Mammoth Mountain towards the Inyo Craters and Domes. These cracks are parallel to the general alignment of

the domes ($\approx N 07^\circ W$). However, structures in the immediate vicinity of the domes and on the surfaces of the domes indicate that the extrusions emerged from elongate conduits oriented approximately $N 05^\circ E$ to $N 15^\circ E$. This relationship may indicate that the domes were fed by a single dike trending NNW that separated into NNE-trending segments as it approached the surface (Fig. 8). Segmentation and change in orientation is a common response of dikes to a systematic change in orientation of the horizontal principal stresses (Delaney and Pollard, 1981). This suggests that dike orientation beneath the Inyo Domes was influenced by local stresses, thus favoring the hypothesis that the dike propagated independently of pre-existing faults and joints.

References Cited

- Anderson, E.M., 1938, Proc. Roy. Soc. Edinburgh, 58, 242.
- Bacon, C.R., Duffield, W.A., and Nakamura, K., 1980, J. Geophys. Res., 85, 2425.
- Bailey, R.A. and Koeppen, 1977, U.S. Geol. Survey Open File Map, 77-468.
- Bailey, R.A., Dalrymple, G.B., and Lanphere, M.A., 1976, J. Geophys. Res., 81, 725.
- Benioff, H. and Gutenberg, B., 1939, Bull. Seism. Soc. Amer., 29, 333.
- Delaney, P.T. and Pollard, D.D., 1981, U.S.G.S. Prof. Paper 1202, 61 p.
- Delaney, P.T. and Pollard, D.D., 1982, Amer. J. Sci., 282, 856.
- Delaney, P.T., Pollard, D.D., Ziony, J.I., and McKee, E.H., 1985, (in prep.)
- Fink, J.H., and Pollard, D.D., 1983a, Geology, 11, 458.
- Fink, J.H., and Pollard, D.D., 1983b, EOS, 64, 898.
- Friedman, M., Handin, J., and Alani, G., 1972, Int. J. Rock Mech. Min. Sci., 9, 757.
- Hill, D.P., 1976, J. Geophys. Res., 81, 745.
- Hoagland, R.G., Hahn, A.R., and Rosenfield, A.R., 1973, Rock Mech., 5, 77.
- Lawn, B.R., and Wilshaw, T.R., 1975, Fracture of Brittle Solids, 204 p.
- McGarr, A.M., 1982, J. Geophys. Res., 87, 9279.
- Nakamura, K., 1977, J. Volc. Geotherm. Res., 2, 1.
- Pollard, D.D., 1973, Tectonophysics, 19, 233.
- Pollard, D.D., Delaney, P.T., Duffield, W.A., Endo, E.T., and Okamura, A.T., 1983, Tectonophysics, 94, 541.
- Rundle, J.B. and Whitcomb, J.H., 1984, (in prep.)
- Sanders, C.O. and Ryall, F., 1983, Geophys. Res. Letters, 10, 2597.
- Savage, J.C. and Cockerham, R.S., 1984, J. Geophys. Res., (in press)
- Savage, J.C. and Clark, M.M., 1982, Science, 217, 531.
- Steeple, D.W. and Iyer, H.M., 1976, J. Geophys. Res., 81, 849.
- Wilson, G., 1970, Geol. Assoc. London Proc., 81, 595.
- Zoback, M.L. and Zoback, M., 1980, J. Geophys. Res., 85, 6113.

Figure Captions

- Figure 1. Plot of stress ratio \underline{R} versus angle α between \underline{x}_1 axis and direction of remote principal stress σ_1^r . Curve separates region where dilation of plane of weakness is possible from region where dilation is not possible by magma at pressure \underline{P}_m .
- Figure 2. Plot of shear to dilational displacement ratio $\underline{u}_2/\underline{u}_1$ versus angle α with stress ratio \underline{R} as parameter. Displacements are calculated at center of dilating plane of weakness.
- Figure 3. Schematic illustration of region near the tip of a vertical dike. Dotted curves outline process zone in which joints form. With continued propagation these joints become adjacent to dike contact.
- Figure 4. Plot of change in horizontal stress σ_{11} from the ambient value σ_{11}^r versus distance perpendicular to dike \underline{x}_1 with distance above dike $\underline{x}_2 - \underline{a}$ as a parameter. Stress is normalized by driving stress $\sigma_{11}^r - \sigma_{11}^c$ and distance by dike half-height \underline{a} .
- Figure 5. Map of sandstone outcrop with vertical dike-parallel joint set and diabase dike. Sandstone is member of Jurassic Summerville Formation in south central Utah.
- Figure 6. Contour map of maximum tensile stress near dike tip at shallow depth. Magma driving pressure is 1 MPa, gravitational gradient is 0.025 MPa/m, and dike is 100 m high. Short dashed lines are perpendicular to contoured stress in region of tension and indicate orientation of possible secondary cracks.
- Figure 7. Plot of spacing between ground cracks \underline{w} versus depth-to-dike-top ($\underline{d} - \underline{a}$), with both distances normalized by depth to dike center \underline{d} . Spacing of the two tensile maxima computed from the elastic model is compared to "rule-of-thumb" estimates.
- Figure 8. Schematic illustration of segmented dike. Arrows indicate rotation of least compressive stress with depth about the dike propagation direction.
- Figure 9. Sketch map of Inyo Domes area showing NNE trend of surficial structures (paired dashed lines) and NNW trend of domes.

Figure 1

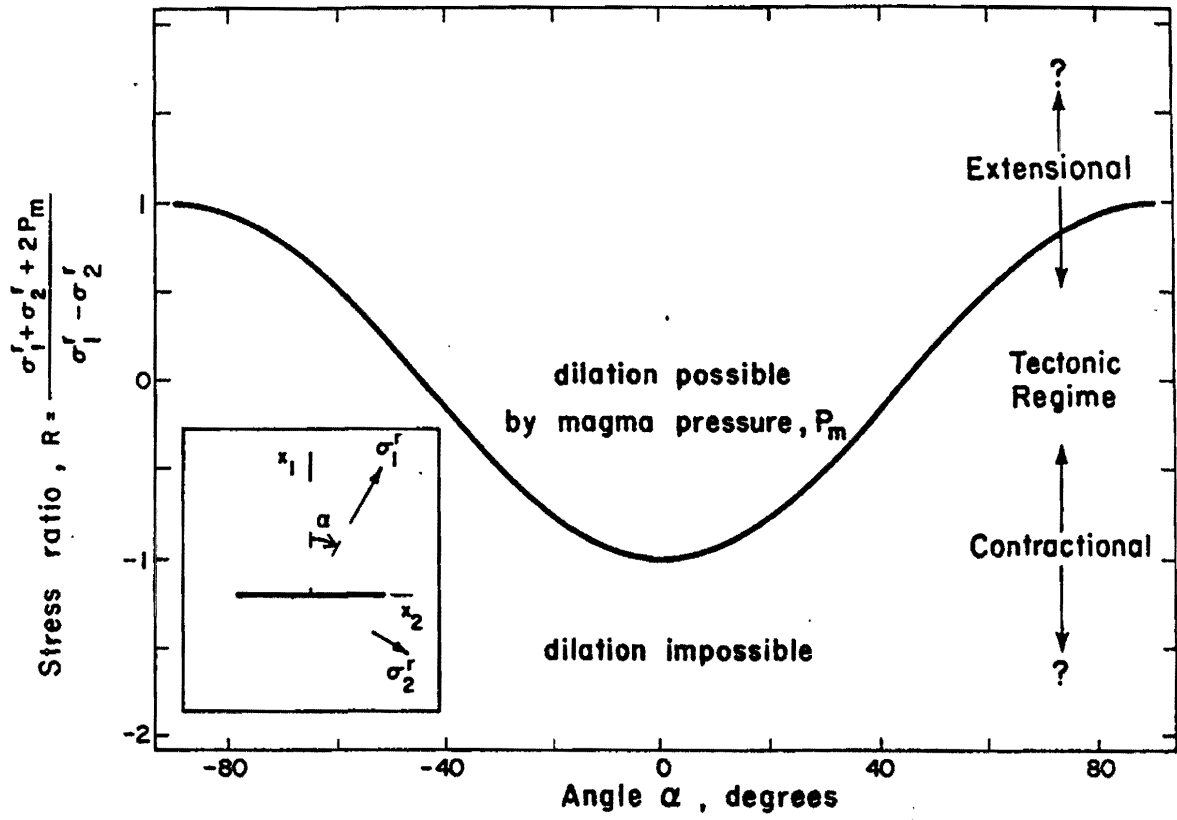


Figure 2

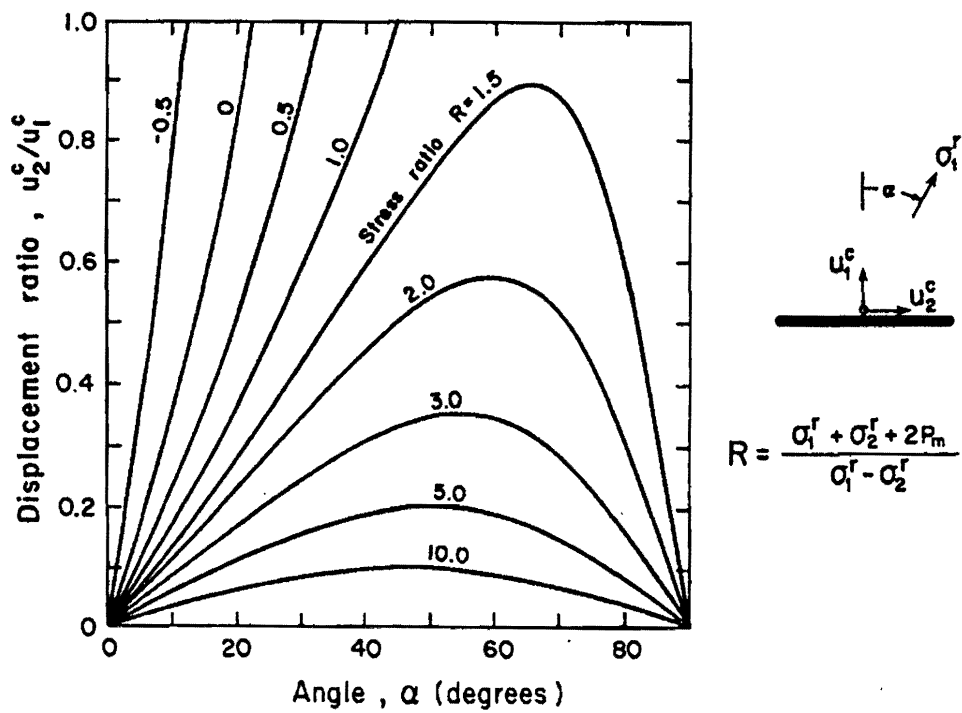


Figure 3

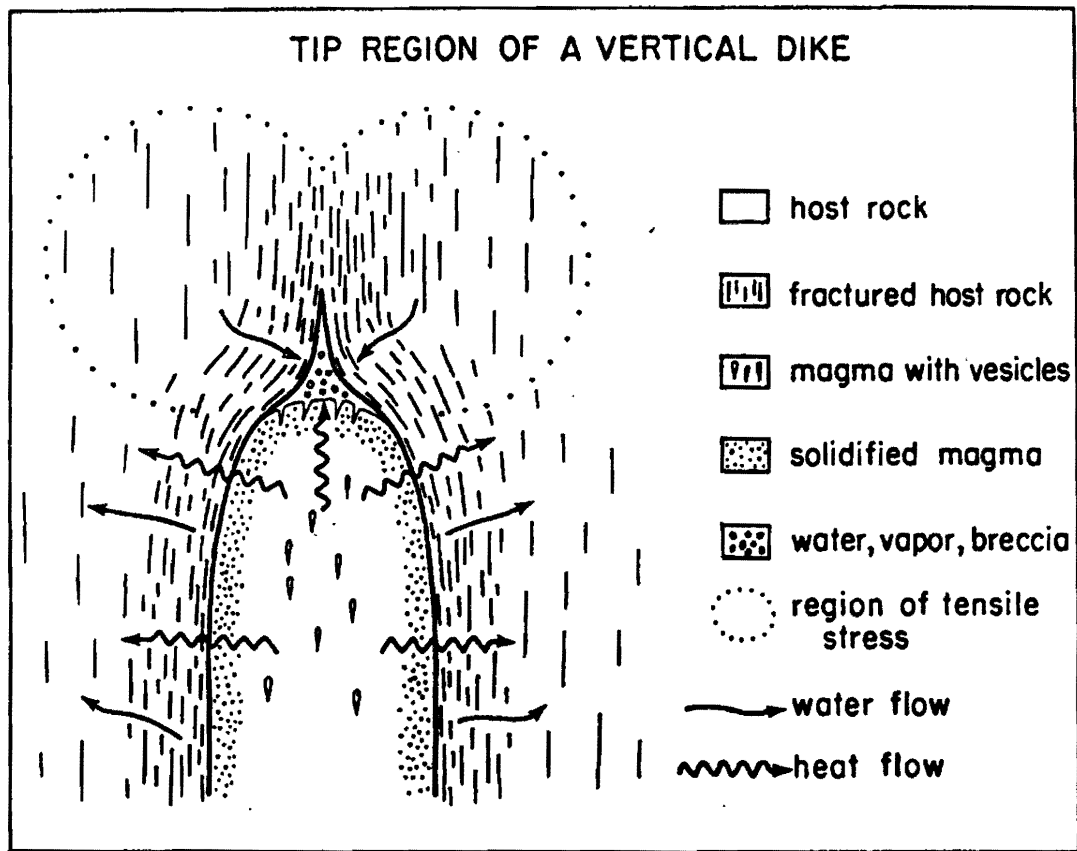


Figure 4

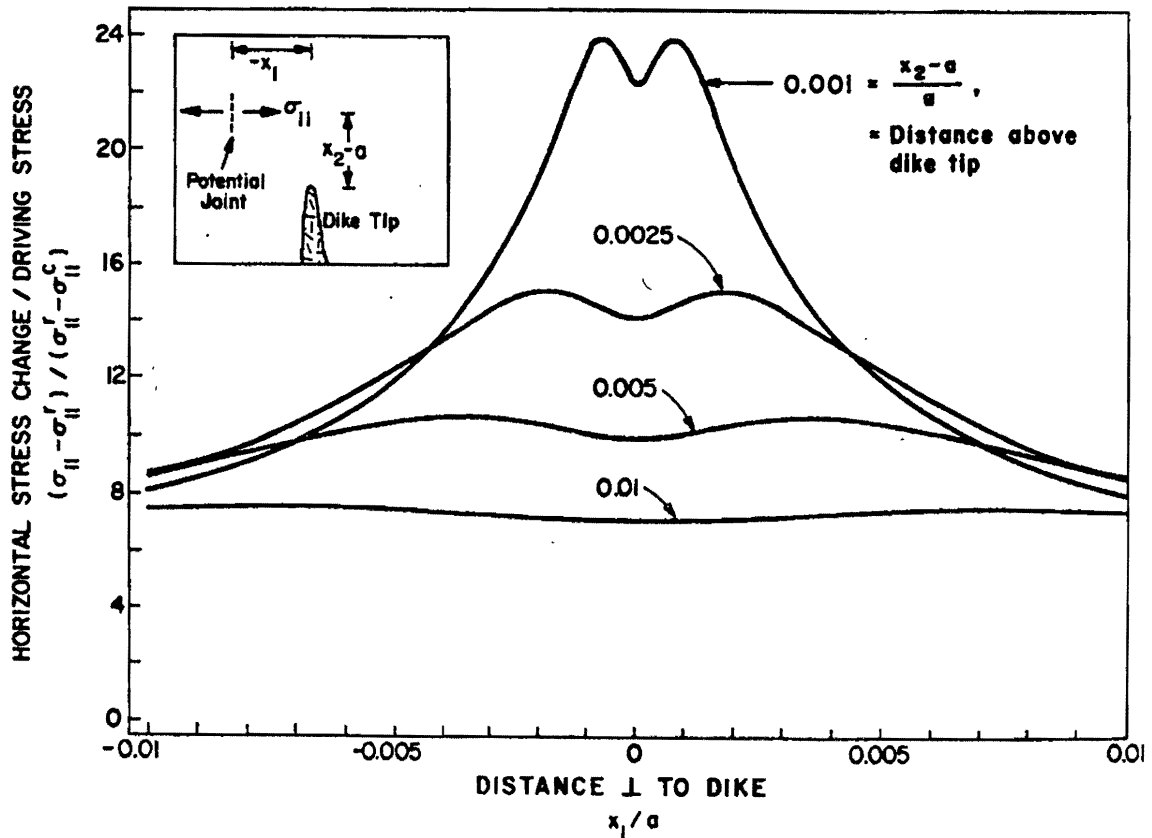


Figure 5

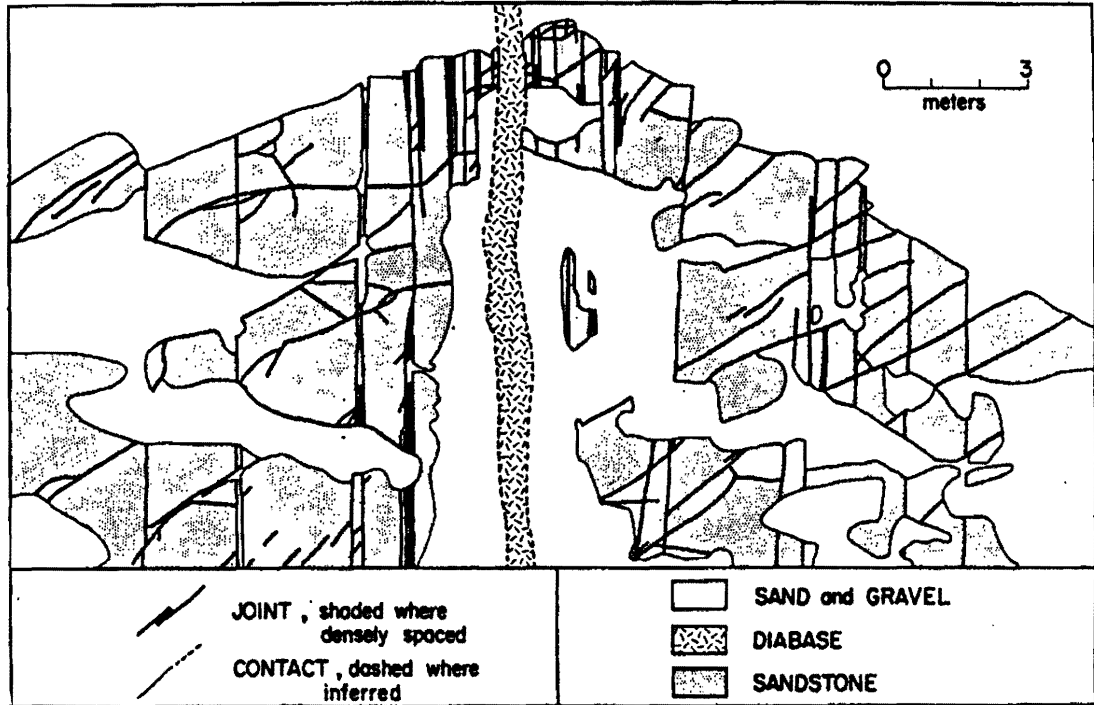


Figure 6

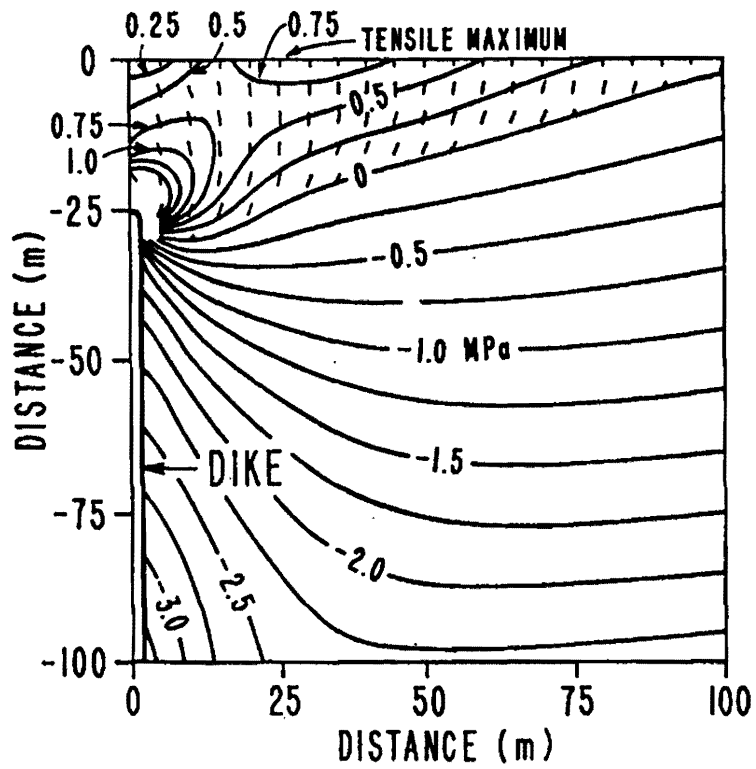


Figure 7

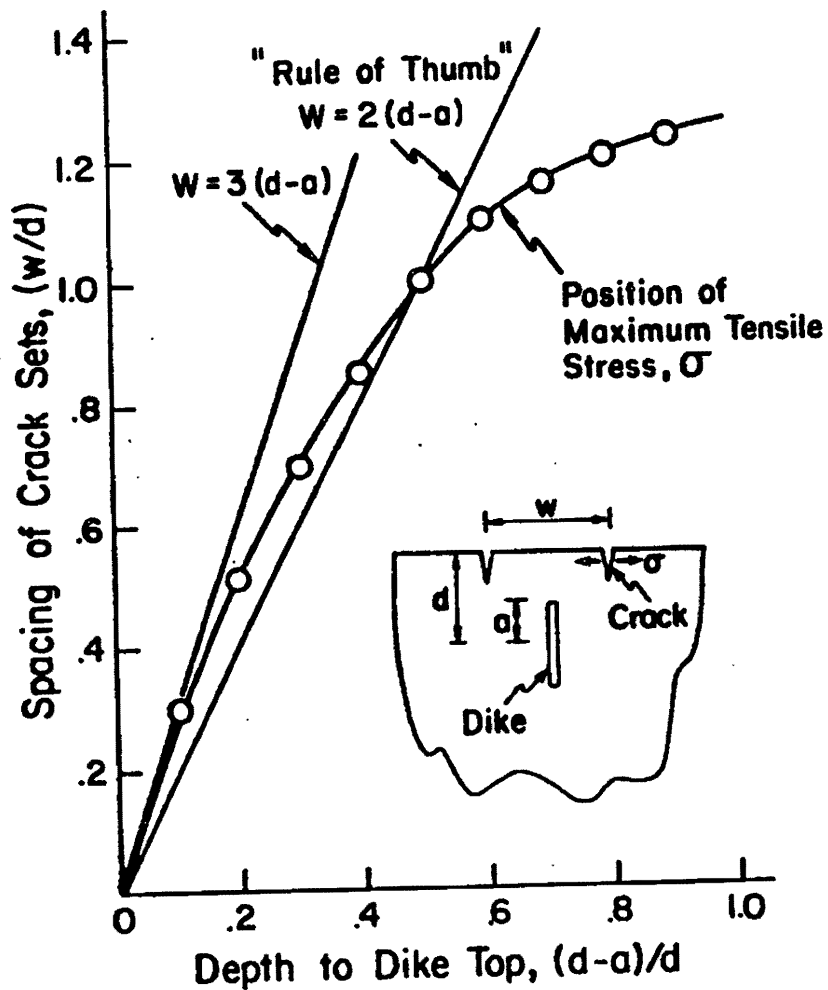


Figure 8

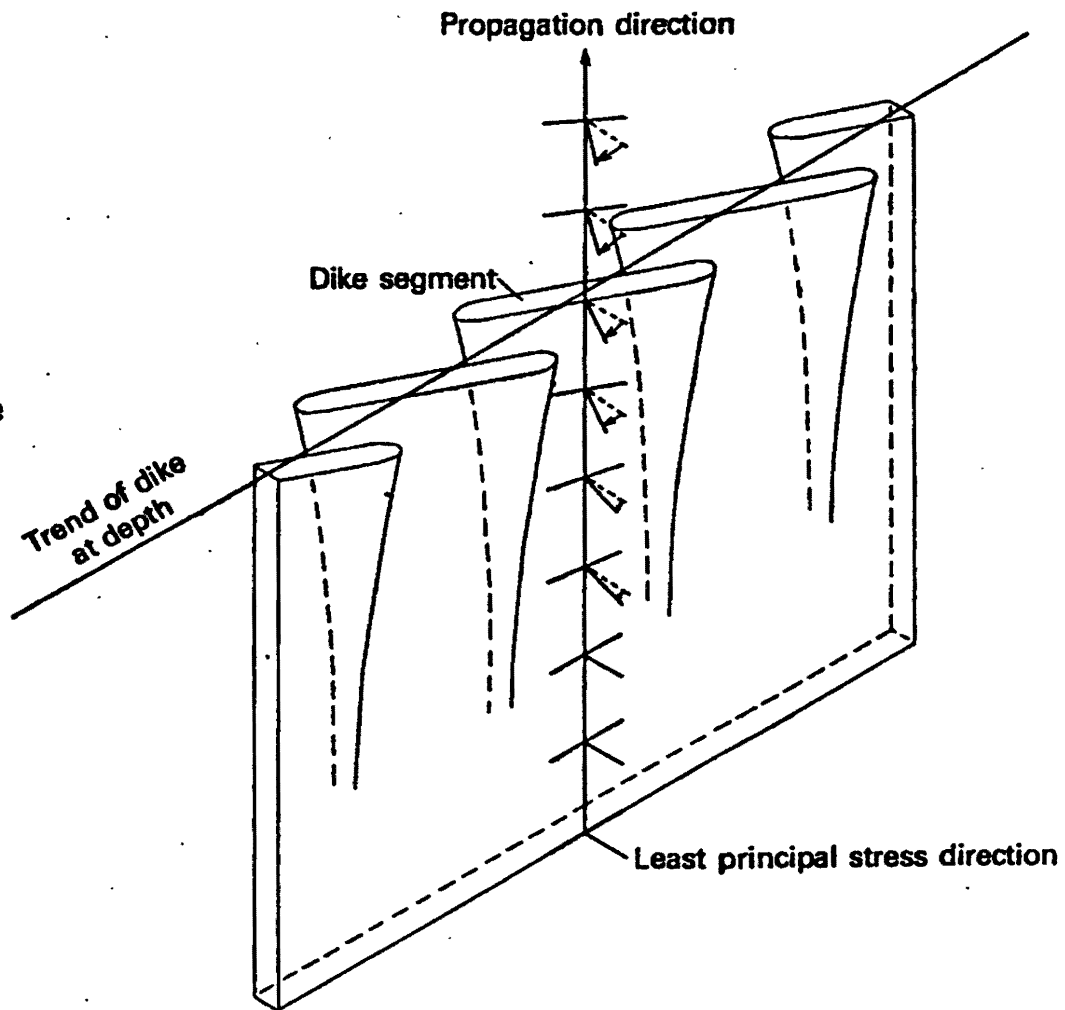


Figure 9

